
Deterministic Uncertainty Propagation for Improved Model-Based Offline Reinforcement Learning

Abdullah Akgül

Department of Mathematics and Computer Science
University of Southern Denmark
Odense, Denmark
akgul@imada.sdu.dk

Manuel Haußmann

Department of Mathematics and Computer Science
University of Southern Denmark
Odense, Denmark
hausmann@imada.sdu.dk

Melih Kandemir

Department of Mathematics and Computer Science
University of Southern Denmark
Odense, Denmark
kandemir@imada.sdu.dk

Abstract

Current approaches to model-based offline Reinforcement Learning (RL) often incorporate uncertainty-based reward penalization to address the distributional shift problem. While these approaches have achieved some success, we argue that this penalization introduces excessive conservatism, potentially resulting in suboptimal policies through underestimation. We identify as an important cause of over-penalization the lack of a reliable uncertainty estimator capable of propagating uncertainties in the Bellman operator. The common approach to calculating the penalty term relies on sampling-based uncertainty estimation, resulting in high variance. To address this challenge, we propose a novel method termed Moment Matching Offline Model-Based Policy Optimization (MOMBO). MOMBO learns a Q-function using moment matching, which allows us to deterministically propagate uncertainties through the Q-function. We evaluate MOMBO's performance across various environments and demonstrate empirically that MOMBO is a more stable and sample-efficient approach.

1 Introduction

Offline reinforcement learning (RL) (Lange et al., 2012; Levine et al., 2020) is a paradigm for extracting the optimal policy from a dataset containing transitions derived from interactions with a behavioral policy in a given environment. This approach proves valuable in various domains where direct interaction with the environment is impractical or risky (Shortreed et al., 2011; Singh et al., 2020; Nie et al., 2021; Micheli et al., 2022). Applying traditional online off-policy RL methods directly to offline RL settings often leads to poor performance due to the distributional shift problem (Fujimoto et al., 2019; Kumar et al., 2019) caused by the accumulation of extrapolation errors during policy evaluation into a positive bias exploited by the policy search step.

It is commonplace to perform offline RL via both model-free and model-based approaches. Model-based offline RL approaches fit a probabilistic model on the real state transitions as a first step and then supplement real data with synthetic samples generated from this model on the fly through the course of policy search (Janner et al., 2019). One line of work addresses distributional shift by constraining the policy learning (Kumar et al., 2019; Fujimoto and Gu, 2021), where the policy is trained to mimic the behavioral policy and penalized based on the discrepancy between its actions and those of the behavioral policy, akin to behavioral cloning. A second strategy is to introduce conservatism to training by (i) perturbing the training objective via a high-entropy behavior policy (Kumar et al., 2020; Yu et al., 2021), (ii) penalizing state-action pairs proportionally to their estimated variance (An et al., 2021; Yu et al., 2020; Bai et al., 2022; Sun et al., 2023), or (iii) adversarially training the dynamics model to minimize the value function (Rigter et al., 2022) to prevent overestimation in policy evaluation for out-of-domain (OOD) state-action pairs.

In the offline RL literature, uncertainty-driven approaches exist for both model-free (An et al., 2021; Bai et al., 2022) and model-based settings (Yu et al., 2020; Sun et al., 2023), all aimed at learning a pessimistic value function (Jin et al., 2021) by penalizing it with an uncertainty estimator. The impact of uncertainty quantification has been investigated in both online (Abbas et al., 2020) and offline (Lu et al., 2021) scenarios, particularly in model-based approaches, which is the setting our work focuses on. Despite model-based research demonstrating the significance of uncertainty estimators and their influence on policy performance, current model-based offline RL methods still lack a reliable uncertainty estimator. These methods struggle to propagate uncertainty from the predicted next state and reward by the learned dynamics model to the Bellman targets, even though policy performance is directly linked to uncertainty in the Bellman error (O’Donoghue et al., 2018; Luis et al., 2023). State-of-the-art approaches (Sun et al., 2023) approximate the variance of Bellman targets by sampling from the learned environment model, which incurs high estimator variance and causes both over-penalization and instability in training.

Our contribution. We identify sampling variance as a common limiting factor for the performance of uncertainty-based model-based offline RL approaches. We characterize the reasons behind this bottleneck by a theoretical analysis of the concentration properties of the estimators in commonplace use. We address this bottleneck by employing progressive moment matching, an idea that has, e.g., useful applications in deterministic variational inference of Bayesian deep learning (Wu et al., 2019a), for the first time to deterministically propagate environment model uncertainties through Q-function estimates. The resulting model, *Moment Matching Offline Model-Based Policy Optimization (MOMBO)*, significantly accelerates training compared to its sampling-based counterparts while maintaining performance. Furthermore, it has favorable theoretical guarantees.

2 Preliminaries

Reinforcement Learning. We define an episodic Markov Decision Process (MDP) as a tuple $\mathcal{M} = (\mathcal{S}, \mathcal{A}, r, T, \gamma, H)$, where \mathcal{S} represents the state space and \mathcal{A} denotes the action space. The function $r(s, a) : \mathcal{S} \times \mathcal{A} \rightarrow [0, R_{\max}]$ is a bounded reward function, and $T(s'|s, a) : \mathcal{S} \times \mathcal{A} \rightarrow \Delta(\mathcal{S})$ represents the state transition probability density where Δ denotes the probability simplex defined on the state space. The parameter $\gamma \in (0, 1)$ is the discount factor and H is the episode length. We define return for a policy π as $J_t(\pi) \triangleq \mathbb{E}_\pi[\sum_{i=t}^H \gamma^{i-t}(s_i, a_i)]$. The objective of RL is to choose a policy that maximizes the cumulative episode reward for the initial state $J_0(\pi)$ within an environment (Sutton and Barto, 2018). Actor-critic algorithms achieve this by alternating between *policy evaluation* and *policy improvement* phases. During the policy evaluation phase, they rely on a deep neural network $Q_\psi^\pi(s_t, a_t) : \mathcal{S} \times \mathcal{A} \rightarrow \mathbb{R}_+ = J_t(\pi)$, to approximate the *Q-function*. The networks parameters ψ are inferred by minimizing the *Bellman error*,

$$\psi^* = \arg \min_{\psi \in \Psi} \mathbb{E}_{(s,a,r,s')} [(Q_\psi^\pi(s, a) - \mathcal{T}^\pi Q_\psi(s, a))^2],$$

where $\mathcal{T}^\pi Q$ is the *Bellman operator*,

$$\mathcal{T}^\pi Q(s_t, a_t) \triangleq r(s_t, a_t) + \gamma \mathbb{E}_{\substack{s_{t+1} \sim T(s_t, a_t) \\ a_{t+1} \sim \pi(a_{t+1}|s_{t+1})}} [Q^\pi(s_{t+1}, a_{t+1})].$$

In the policy improvement phase, actor-critic algorithms learn a policy using a deep neural network parameterized by ξ through maximizing the Q-value: $\xi^* = \arg \min_{\xi \in \Xi} \mathbb{E}_s [-Q_{\psi^*}^{\pi_\xi}(s, \pi_\xi(a|s))]$.

Model-based offline RL algorithms. Offline RL algorithms perform policy search using only a dataset $\mathcal{D} = \{(s_i, a_i, r_i, s'_i)\}_{i=1}^{|\mathcal{D}|}$ collected from the target environment beforehand by a behavioral policy π_β . Unlike online RL, the policy search algorithm does not interact with the environment during training. In model-based approaches for offline RL, a dynamics model \hat{T} is commonly trained through maximum likelihood estimation (MLE) using the provided dataset \mathcal{D} , i.e., $\min_{\hat{T}} \mathbb{E}_{s,a,s' \sim \mathcal{D}} [-\log \hat{T}(s'|s,a)]$. Additionally, a reward model $\hat{r}(s,a)$ can also be jointly trained using \mathcal{D} . Together, these models form an estimated MDP, $\hat{\mathcal{M}} = \{\mathcal{S}, \mathcal{A}, \hat{r}, \hat{T}, \gamma, H\}$. Subsequently, an optimal policy can be learned from $\hat{\mathcal{M}}$ through planning or RL algorithms. Mainstream model-based offline RL methods adopt the Dyna approach (Sutton, 1990; Janner et al., 2019), which suggests training an off-the-shelf model-free RL algorithm on synthetic data generated from the learned environment model $\hat{\mathcal{D}}$ using initial states from \mathcal{D} . It has been observed that shuffling minibatches collected from synthetic and real data sets improves performance in both online (Janner et al., 2019) and offline (Yu et al., 2020) settings. The state-of-the-art approach models state transition probabilities and reward distributions as an ensemble (Lakshminarayanan et al., 2017) of N_{ens} heteroscedastic neural networks assuming a normal density.

3 Limitations of SOTA model-based offline RL approaches

Offline RL methods face the primary challenge of *distributional shift* because the static dataset lacks coverage of a large portion of the state-action space. When the policy search algorithm probes unobserved state-action pairs in the course of training, significant value approximation errors occur. While in standard supervised learning scenarios these errors shrink as the model observes more data, in RL, overestimation errors are picked up during the policy improvement step and stay within the system causing the well-known *overestimation bias* (Thrun and Schwartz, 1993). While this issue can be mitigated in online setups by min-clipping (Fujimoto et al., 2018), additional measures are required in offline RL setups, such as adding penalties to rewards proportional to the uncertainty around the next state estimates. Algorithms belonging to this family, known commonly as *pessimistic policy iteration* (Yu et al., 2020; Sun et al., 2023), build on a theory that provides performance improvement guarantees for an upper bound on the next state variance (Jin et al., 2021; Uehara and Sun, 2022). The state-of-the-art practice exploits the fact that the theoretical guarantees are tighter when applied on the uncertainty of the value estimate of the next state, rather than the next state itself (Sun et al., 2023). When deep neural networks are used as value function approximators, calculating their variance even for normal distributed input becomes analytically intractable. Hence, reward penalties are obtained by Monte Carlo samples, which are prone to high estimator variance.

It is our key finding that using high-variance estimates for reward penalization causes three significant problems in the training process of offline RL algorithms:

- (i) The information content of the distorted gradient signal shrinks, causing delayed convergence to the asymptotic performance.
- (ii) The first two moments of the Bellman target are poorly approximated for reasonable sample counts.
- (iii) Excessively large confidence radii need to be used to counter the instability caused by (i) and the high overestimation risk caused by the inaccuracy described in (ii), which restricts model capacity at unnecessary levels.

We propose a novel approach centered on deterministic uncertainty propagation using moment-matching, originally developed for Bayesian inference, combined with a lower confidence bound. Through moment matching, we can effectively propagate uncertainty from the predictions of the dynamics to the Q-function without encountering the high variance caused by sampling errors. By employing a robust uncertainty estimator, we establish a lower confidence bound on the target Q-value, enabling a more efficient, sampling-free penalization with improved training times.

The common practice in model-based offline RL algorithms is to generate imaginary rollouts at every episode start. The generated data are shuffled with the real observations and used to update the policy. During this generation process, samples from the predictive distributions of the next state and reward are used. These predicted samples are later used again to calculate the Bellman error when updating the Q-function. However, estimators calculated from these samples are subject to

sampling errors, which may amplify overestimation biases. To address these sampling errors and to tackle distributional shift, model-based offline RL methods often adopt conservative policies and penalize the state-action values based on the target predictions. The target Q-value ($\mathcal{T}^\pi Q(s, a)$) for the model-based offline RL algorithm is

$$\mathcal{T}^\pi Q(s, a) = \mathbb{E}_{\substack{r \sim \widehat{r}(s, a) \\ s' \sim \widehat{\mathbb{T}}(s' | s, a)}} [r + \gamma \mathbb{E}_{a' \sim s'} [Q^\pi(s', a')]], \quad (1)$$

where $\widehat{\mathbb{T}}$ and \widehat{r} are learned transition and reward models respectively. Despite various options for conservatism in the model-based offline RL literature, such as reward penalization by prediction uncertainty of the dynamics model (Yu et al., 2020; Lu et al., 2021), or by using uncertainty on the Q-value of the next state by taking samples (Sun et al., 2023), there is no analytical solution. Furthermore, these uncertainty estimators are not able to accurately reflect the real uncertainty on the target Q-value because they cannot propagate the uncertainty through the Q-function. Instead, they have to approximate it by taking samples, which incurs high estimator variance, leading to over-penalization and limiting the learning speed. In the following section, we provide a theoretical analysis of sampling-based uncertainty estimation and present a tail bound for one of the most successful state-of-the-art methods, namely MOBILE (Sun et al., 2023).

We assume that the estimation error surrounding the Bellman target estimate of a state-action pair is normally distributed $y \sim \mathcal{N}(\mu, \sigma^2)$. The lower bound of a confidence set surrounding its mean is then given as $y = \mu - \beta\sigma$ for some radius $\beta > 0$. We refer to this quantity as a β -Lower Confidence Bound (β -LCB). For a sample $S = \{y_1, \dots, y_N\}$ of N independently identically distributed (i.i.d.) draws from this distribution, denote the empirical estimate of the β -LCB as $\widehat{y}_s \triangleq \widehat{\mu}_N - \beta\widehat{\sigma}_N$ for the empirical mean and variance estimates

$$\widehat{\mu}_N \triangleq \frac{1}{N} \sum_{n=1}^N y_n, \quad \widehat{\sigma}_N^2 \triangleq \frac{\sum_{i=1}^N (y_i^2 - \widehat{\mu}_N)}{N-1}. \quad (2)$$

Offline RL algorithms that apply pessimism to their target Q-value estimate use a β -LCB estimate. E.g., the target Q-value estimate of MOBILE (Sun et al., 2023) can be expressed as $\widehat{y}_s \triangleq \widehat{\mu}_N - \beta\widehat{\sigma}_N$, which is a β -LCB estimate, where

$$\widehat{\mu}_N = r + \gamma(1-d)Q^\pi(s', a'), \quad \widehat{\sigma}_N = \sqrt{\text{var}[Q^\pi(s', a')]}.$$
 (3)

We discuss additional work related to our proposal in Appendix A.

4 MOMBO: Moment matching offline model-based policy optimization

Deterministic uncertainty propagation via moment matching. To compute target Q-values for the synthetic dataset one needs to perform mathematical operations on uncertain inputs. Typically, the impact of uncertain inputs on the output is approximated by sampling and evaluation. However, this method introduces sampling errors and computational overhead. We propose to instead propagate uncertainty through Q-function operations using moment matching. Moment matching-based uncertainty propagation offers better accuracy, computational efficiency, and reduces estimator variance (Wu et al., 2019a; Wang and Manning, 2013).

Assuming the input of a fully-connected layer to be $X \sim \mathcal{N}(X|\mu, \sigma^2)$, the pre-activation Y for a neuron associated with weights θ , is given as $Y = \theta^\top X$, i.e., $Y \sim \mathcal{N}(Y|\theta^\top \mu, (\theta^2)^\top \sigma^2)$, where we absorbed the bias into θ for simplicity and the square on θ is applied element-wise. For a ReLU activation function $r(x) \triangleq \max(0, x)$, mean $\widetilde{\mu}$ and variance $\widetilde{\sigma}^2$ of $Y = \max(0, X)$ are analytically tractable (Frey and Hinton, 1999). We approximate the output with a normal distribution, $\widetilde{X} \sim \mathcal{N}(\widetilde{X}|\widetilde{\mu}, \widetilde{\sigma}^2)$, and summarize several properties about $\widetilde{\mu}$ and $\widetilde{\sigma}^2$ below.

Lemma 1 (Moment matching). For $X \sim \mathcal{N}(X|\mu, \sigma^2)$ and $Y = \max(0, X)$, we have

$$(i) \quad \begin{aligned} \widetilde{\mu} &\triangleq \mathbb{E}[Y] = \mu\Phi(\alpha) + \sigma\phi(\alpha), \\ \widetilde{\sigma}^2 &\triangleq \text{var}[Y] = (\mu^2 + \sigma^2)\Phi(\alpha) + \mu\sigma\phi(\alpha) - \widetilde{\mu}^2, \end{aligned}$$

where $\alpha = \mu/\sigma$, and $\phi(\cdot)$, $\Phi(\cdot)$ are the probability density function (pdf) and cumulative distribution function (cdf) of the standard normal distribution, respectively. Additionally, we have that

$$(ii) \quad \widetilde{\mu} \geq \mu \quad \text{and} \quad (iii) \quad \widetilde{\sigma}^2 \leq \sigma^2.$$

We can show the following inequality between the cdfs, $F_U(u) \triangleq \mathbb{P}(U \leq u)$, of X and \tilde{X} .

Lemma 2 (An inequality between normal cdfs). *For two normally distributed random variables $X \sim \mathcal{N}(X|\mu, \sigma^2)$ and $\tilde{X} \sim \mathcal{N}(\tilde{X}|\tilde{\mu}, \tilde{\sigma}^2)$ with $\tilde{\mu}\sigma \geq \mu\tilde{\sigma}$, the following inequality holds:*

$$F_{\tilde{X}}(u) \leq F_X(u), \quad \text{for } u \leq 0.$$

Given $\tilde{\mu}$ and $\tilde{\sigma}^2$ as in Lemma 1, the assumptions of this lemma hold and it is applicable to our moment-matching propagation. See Appendix B for proofs on these two lemmata.

As the input to our Q-function, which propagates uncertainties deterministically through moment matching, we provide a distribution of the next state, with known mean and variance as predictions of the dynamics model, along with an action sampled from the policy for the mean of the next state and a zero variance. I.e., we treat the action as if it followed a delta distribution and simply propagate its mean throughout the neural net. The moment matching procedure is outlined in Algorithm 1.

Algorithm 1 Deterministic uncertainty propagation through moment matching

```

function MOMENTMATCHINGTHROUGHLINEAR( $\theta, b, X$ )
   $\theta$ : Weights of the layer,  $b$ : bias of the layer
   $X = \mathcal{N}(X|\mu_X, \sigma_X^2)$  ▷ input a normal distribution
   $(\mu_Y, \sigma_Y^2) \leftarrow (\theta^\top \mu_X + b, \theta^{2\top} \sigma_X^2)$  ▷ transform mean and variance
  return  $Y = \mathcal{N}(X|\mu_Y, \sigma_Y^2)$  ▷ output the transformed distribution
end function

function MOMENTMATCHINGTHROUGHRELU( $X$ )
   $X = \mathcal{N}(X|\mu_X, \sigma_X^2)$  ▷ input a normal distribution
   $\alpha \leftarrow \mu_X / \sigma_X$ 
   $\mu_Y \leftarrow \mu_X \Phi(\alpha) + \sigma_X \phi(\alpha)$  ▷ compute the first two moments of ReLU( $X$ )
   $\sigma_Y^2 \leftarrow (\mu_X^2 + \sigma_X^2) \Phi(\alpha) + \mu_X \sigma_X \phi(\alpha) - \mu_Y^2$  ▷  $\phi/\Phi$  are the normal pdf/cdf
  return  $Y = \mathcal{N}(X|\mu_Y, \sigma_Y^2)$  ▷ output a normal distribution with these moments
end function

```

Lower confidence bound on target Q-value. We construct a lower confidence bound on the target Q-value (Equation (1)) by representing it as a normally distributed random variable. We use ensemble dynamics models, reward models, and a value function capable of propagating an input distribution to the output in order to construct this LCB. Leveraging moment matching on the value function and ensemble dynamics models, the target Q-value can be expressed as a summation of normal distributions without requiring samples. We formulate the β -LCB for MOMBO as

$$\hat{\mu} = \frac{1}{N} \sum_{n=1}^N \mu_r^n + \gamma \mu_{Q'}^n, \quad \hat{\sigma} = \sqrt{\frac{1}{N} \sum_{n=1}^N \left((\mu_r^n + \gamma \mu_{Q'}^n) - \hat{\mu} \right)^2},$$

where N is the number of learned transition models,

$$\begin{aligned} \hat{r}(s, a) &= \mathcal{N}(\mu_r^n, (\sigma_r^n)^2), & \hat{\mathbb{T}}(s'|s, a) &= \mathcal{N}(\mu_{s'}^n, (\sigma_{s'}^n)^2), \\ Q' &= \mathcal{N}(\mu_{Q'}^n, (\sigma_{Q'}^n)^2) = f_L(\mathcal{N}(\mu_{s'}^n, (\sigma_{s'}^n)^2), a^n), \end{aligned}$$

and $a^{ln} \sim \pi(a^{ln}|\mu_{s'}^n)$. Our pessimistic target Q-value estimate of MOMBO is $\mathcal{T}^\pi Q(s, a) = \hat{\mu} - \beta \hat{\sigma}$.

4.1 Practical implementation of MOMBO

We adopt the model learning scheme from model-based policy optimization (MBPO) (Janner et al., 2019) and use Soft Actor-Critic (SAC) (Haarnoja et al., 2018) as the policy search algorithm, as these are the best practices used in many recent model-based offline RL methods (Yu et al., 2020, 2021; Sun et al., 2023). However, we note that most of our findings are more broadly applicable.

Following MBPO, we train an independent neural ensemble of dynamics models. These models output Gaussian distributions over the next state and reward via MLE. We denote each member of the ensemble as $\hat{\mathbb{T}}^i(s', r|s, a) = \mathcal{N}(\mu^i(s, a), (\sigma^i)^2(s, a))$ for $i \in \{1, \dots, N_{\text{ens}}\}$. After evaluating their

performance on a validation set, we select the N_{elite} best-performing ensemble elements for further processing. These elite models are used for generating k -step rollouts with the current policy to create the synthetic dataset $\widehat{\mathcal{D}}$, which we then combine with the offline dataset \mathcal{D} . Additionally, we construct LCB on the target Q-value. For clarity, we distinguish the dynamics model and reward model separately as $\widehat{T}^i(s'|s, a) = \mathcal{N}(\mu_{s'}^i, (\sigma_{s'}^i)^2)$ and $\widehat{r}^i(r|s, a) = \mathcal{N}(\mu_r^i, (\sigma_r^i)^2)$ for $i \in \{1, \dots, N_{\text{elite}}\}$.

For policy learning, we modify SAC and switch its Q-function approximator, which is a neural network, with our proposed deterministic moment propagating neural network. Additionally, we add a pessimistic target Q-value calculation. The critic networks $Q_{\psi_k}^{\pi_\xi}(\cdot, \cdot)$ for the policy π_ξ are trained with the following loss

$$\mathcal{L}(Q_{\psi_k}^{\pi_\xi}) = \mathbb{E}_{(s,a,r,s') \sim \mathcal{D} \cup \widehat{\mathcal{D}}} \left[\left(\mu_{Q_{\psi_k}^{\pi_\xi}} - \mathcal{T}^{\pi_\xi} Q(s, a) \right)^2 \right], \quad \text{for } k = 1, 2, \quad (4)$$

where we use the mean of the Q-value distribution $Q_{\psi_k}^{\pi_\xi}(s, a) = \mathcal{N}(\mu_{Q_{\psi_k}^{\pi_\xi}}, \sigma_{Q_{\psi_k}^{\pi_\xi}}^2)$. The target is

$$\mathcal{T}^{\pi_\xi} Q(s, a) = \begin{cases} r + \gamma \mathbb{E}_{a' \sim \pi_\xi(a'|s')} \left[\min_{k=1,2} Q_{\bar{\psi}_k}^{\pi_\xi}(s', a') \right], & (s, a, r, s') \in \mathcal{D} \\ \widehat{\mu} - \beta \widehat{\sigma}, & (s, a, r, s') \in \widehat{\mathcal{D}}, \end{cases}$$

where $\bar{\psi}_k$ indicates that it is not updated during a stochastic gradient update. Additionally,

$$\widehat{\mu} = \frac{1}{N_{\text{elite}}} \sum_{i=1}^{N_{\text{elite}}} \mu_r^i + \gamma \mathbb{E}_{a' \sim \pi_\xi(a'|s')} \left[\min_{k=1,2} \mu_{Q_{\bar{\psi}_k}^{\pi_\xi, i}} \right],$$

and

$$\widehat{\sigma} = \sqrt{\frac{1}{N_{\text{elite}}} \sum_{i=1}^{N_{\text{elite}}} \left(\left(\mu_r^i + \gamma \mathbb{E}_{a' \sim \pi_\xi(a'|s')} \left[\min_{k=1,2} \mu_{Q_{\bar{\psi}_k}^{\pi_\xi, i}} \right] \right) - \widehat{\mu} \right)^2}.$$

Finally, we choose the policy π_ξ by optimizing

$$\mathcal{L}(\pi_\xi) = -\mathbb{E}_{s \sim \mathcal{D} \cup \widehat{\mathcal{D}}} \left[\min_{k=1,2} Q_{\psi_k}^{\pi_\xi}(s, a) - \alpha \log \pi_\xi(a|s) \right], \quad (5)$$

where α is either a fixed or learnable hyperparameter.

4.2 Theoretical analysis

The key outcome of this analysis is that it is easier to obtain tight upper bounds on value approximation errors using moment matching (Theorem 2) compared to Monte Carlo sampling (Theorem 1). We provide proofs for all statements in this section in Appendix B.

We evaluate the approximation error in terms of the Wasserstein distance, which is defined as follows.

Definition 1 (Wasserstein distance). Let (M, d) denote a metric space, and let $p \in [1, \infty]$. The Wasserstein p -distance between two probability measures ρ_1 and ρ_2 on M , with finite p -moments, is

$$W_p(\rho_1, \rho_2) \triangleq \inf_{\gamma \in \Gamma(\rho_1, \rho_2)} \left(\mathbb{E}_{(x,y) \sim \gamma} [d(x, y)^p] \right)^{1/p}, \quad (6)$$

where $\Gamma(\cdot, \cdot)$ represents the set of all couplings of the two measures, ρ_1 , and ρ_2 .

For $p = 1$, the Wasserstein 1-distance, W_1 , can be simplified (see, e.g., Villani et al., 2009) to

$$W_1(\rho_1, \rho_2) = \int_{\mathbb{R}} |F_1(x) - F_2(x)| d(x). \quad (7)$$

where ρ_1, ρ_2 are two probability measures on \mathbb{R} and $F_1(\cdot), F_2(\cdot)$, their respective cdfs.

Given this definition, we can prove the following two bounds on W_1 .

Lemma 3 (Wasserstein inequalities). The following inequalities hold for the 1-Wasserstein metric

$$(i) \quad W_1(\rho_U^1, \rho_U^2) \leq \|A\|_1 W_1(\rho_V^1, \rho_V^2), \text{ for } U = AV + b, \text{ where } \|\cdot\| \triangleq \|\cdot\|_1 \text{ is the 1-norm.}$$

(ii) $W_1(\rho_Z^1, \rho_Z^2) \leq W_1(\rho_U^1, \rho_U^2)$, for $Z = f(U)$ with $f(\cdot)$ locally K -Lipschitz with $K \leq 1$,

where ρ_x is the density of x , $U \in \mathbb{R}^{d_u}$, $V \in \mathbb{R}^{d_v}$, $A \in \mathbb{R}^{d_u \times d_v}$, and $b \in \mathbb{R}^{d_u}$.

That is, for a fully connected linear layer with ReLU activation function, a 1-Lipschitz mapping, we have an analytical upper bound. We generalize this to an L layer multi-layer perceptron (MLP).

Lemma 4 (W_1 bound on an MLP). *Consider a MLP $f(\cdot)$ with L layers*

$$Y_l = A_l^\top X_{l-1} + b_l, \quad X_l = r(Y_l) \quad l = 1, \dots, L,$$

where A_l, b_l are the weight matrix and bias vector for layer l , and $r(\cdot)$ denotes an elementwise 1-Lipschitz activation function. We write $Y \triangleq Y_L = f(X_0)$, where X_0 is the input. Assuming two measures $X_1 \sim \rho_X^1$ and $X_2 \sim \rho_X^2$, we have that

$$W_1(\rho_Y^1, \rho_Y^2) \leq \prod_{l=1}^L \|A_l\| W_1(\rho_X^1, \rho_X^2).$$

I.e., the W_1 distance between two measures on the output distribution is upper bounded by the W_1 distance between the corresponding input measures with a factor given by the product of the norms of the weight matrices A_l . This result allows us to provide a probabilistic bound on the W_1 distance between a normal ρ_Y and its empirical, sampling-based, estimate $\hat{\rho}_Y$.

Theorem 1 (*Sampling-based MLP bound*). *For an L layer MLP $f(\cdot)$ as defined in Lemma 4, with $Y \triangleq Y_L = f(X)$ where $X \sim \mathcal{N}(X|\mu_X, \sigma_X^2)$, the following bound holds:*

$$\mathbb{P} \left(W_1(\rho_Y, \rho_Y^N) \leq \prod_{l=1}^L \|A_l\| \sqrt{-\frac{8 \log(\delta/4) R_{\max}^2}{\lfloor N/2 \rfloor (1-\gamma)^2}} \right) \geq 1 - \delta.$$

where $\delta \in (0, 1)$ and $\hat{\rho}_Y^N$ is the empirical estimate given N i.i.d. samples.

While Lemma 3 focused on generic densities and the relation between their W_1 distances, we can prove a concrete, analytical bound for our specific moment-matching pipeline. In this case, we bound the W_1 distance between the true density ρ_Y and its moment-matching approximation $\rho_{\tilde{Y}}$.

Lemma 5 (*Moment-matching bound*). *For the following three random variables*

$$X \sim \rho_X, \quad Y = \max(0, X), \quad \tilde{X} \sim \mathcal{N}(\tilde{X}|\tilde{\mu}, \tilde{\sigma}^2),$$

with $\tilde{\mu} = \mathbb{E}[Y]$ and $\tilde{\sigma}^2 = \text{var}[Y]$ the following inequality holds

$$W_1(\rho_Y, \rho_{\tilde{X}}) \leq \int_{-\infty}^0 F_{\tilde{X}}(u) du + W_1(\rho_X, \rho_{\tilde{X}}).$$

If $\rho_X = \mathcal{N}(X|\mu, \sigma)$, it can be further simplified to

$$W_1(\rho_Y, \rho_{\tilde{X}}) \leq \tilde{\sigma} \phi\left(\frac{\tilde{\mu}}{\tilde{\sigma}}\right) - \tilde{\mu} \Phi\left(-\frac{\tilde{\mu}}{\tilde{\sigma}}\right) + |\mu - \tilde{\mu}| + |\sigma - \tilde{\sigma}|.$$

where $\Phi(\cdot)$ is the cdf of a standard normal distribution.

Applying this to moment-matching MLP with L layers, we get the following deterministic bound.

Theorem 2 (*Moment-matching MLP bound*). *Let $f(X)$, be an MLP with L fully connected layers, and ReLU activation $r(x) = \max(0, x)$. For $l = 1, \dots, L-1$, the sampling-based forward-pass is*

$$Y_0 = X_s, \quad Y_l = r(f_l(Y_{l-1})), \quad Y_L = f_L(Y_{L-1}),$$

where $f_l(\cdot)$ is the l -th layer and X_s a sample of $\mathcal{N}(X|\mu_X, \sigma_X^2)$. Its moment matching pendant is

$$\tilde{X}_0 \sim \mathcal{N}(\tilde{X}_0|\mu_X, \sigma_X^2), \quad \tilde{X}_l \sim \mathcal{N}\left(\tilde{X}_l \mid \mathbb{E}\left[r(f_l(\tilde{X}_{l-1}))\right], \text{var}\left[r(f_l(\tilde{X}_{l-1}))\right]\right).$$

The following inequality holds for $\tilde{\rho}_Y = \rho_{\tilde{X}_L} = \mathcal{N}(\tilde{X}_L | \mathbb{E}[f(\tilde{X}_{L-1})], \text{var}[f(\tilde{X}_{L-1})])$.

$$W_1(\rho_Y, \tilde{\rho}_Y) \leq \sum_{l=2}^L (G(\tilde{X}_{l-1}) + C_{l-1}) \prod_{j=1}^L \|A_j\|,$$

Table 1: Normalized reward at 3M gradient steps and Area Under the normalized reward Curve (AUC) (mean \pm std) scores are averaged across four repetitions for the MuJoCo domain of the D4RL offline RL dataset. The highest normalized reward and AUC scores are highlighted in bold and are underlined if they fall within one standard deviation of the best score. The average normalized score is the average across all tasks, and the average ranking is calculated based on the rank of the mean.

Dataset Type	Environment	NORMALIZED REWARD (\uparrow)			AUC (\uparrow)		
		MOPO	MOBILE	MOMBO	MOPO	MOBILE	MOMBO
random	halfcheetah	37.2 \pm 1.6	41.2 \pm 1.1	43.6\pm1.1	36.3 \pm 1.0	39.5 \pm 1.2	41.4\pm1.0
	hopper	31.7\pm0.1	31.3 \pm 0.1	25.4 \pm 10.2*	28.6\pm1.4	23.6 \pm 3.7	17.3 \pm 1.3
	walker2d	8.2 \pm 5.6	22.1\pm0.9	<u>21.5\pm0.1</u>	5.4 \pm 3.2	18.0 \pm 0.4	19.2\pm0.5
medium	halfcheetah	72.4 \pm 4.2	<u>75.8\pm0.8</u>	76.1\pm0.8	70.9 \pm 2.0	<u>72.1\pm1.0</u>	73.0\pm0.9
	hopper	62.8 \pm 38.1	103.6 \pm 1.0	104.2\pm0.5	37.0 \pm 15.3	<u>82.2\pm7.3</u>	95.9\pm2.5
	walker2d	85.4 \pm 2.9	88.3\pm2.5	<u>86.4\pm1.2</u>	77.6 \pm 1.3	79.0 \pm 1.3	84.0\pm1.1
medium-replay	halfcheetah	72.1\pm3.8	<u>71.9\pm3.2</u>	<u>72.0\pm4.3</u>	68.4 \pm 4.7	67.9 \pm 2.8	68.7\pm3.9
	hopper	92.7 \pm 20.7	105.1\pm1.3	<u>104.8\pm1.0</u>	81.7 \pm 4.6	78.7 \pm 4.0	87.3\pm2.0
	walker2d	85.9 \pm 5.3	90.5\pm1.7	<u>89.6\pm3.8</u>	65.3 \pm 12.7	<u>79.9\pm4.3</u>	80.8\pm5.6
medium-expert	halfcheetah	83.6 \pm 12.5	100.9 \pm 1.5	103.3\pm0.8	77.1 \pm 4.0	94.5 \pm 1.8	95.2\pm0.7
	hopper	74.9 \pm 44.2	<u>112.5\pm0.2</u>	112.6\pm0.3	55.6 \pm 17.3	<u>82.7\pm7.3</u>	84.3\pm4.7
	walker2d	108.2 \pm 4.3	114.5\pm2.2	<u>113.9\pm0.9</u>	88.3 \pm 6.3	94.3 \pm 0.9	98.9\pm3.3
Average Normalized Reward		67.9	79.8	79.4	57.7	67.7	70.5
Average Ranking		2.7	1.7	1.7	2.7	2.2	1.2

*High standard deviation due to failure in one repetition, which can be mitigated by increasing β . Median result: 31.3

$$\text{with } G(\tilde{X}_l) = \tilde{\sigma}_l \phi\left(\frac{\tilde{\mu}_l}{\tilde{\sigma}_l}\right) - \tilde{\mu}_l \Phi\left(-\frac{\tilde{\mu}_l}{\tilde{\sigma}_l}\right) \leq 1, \quad C_l \leq |A_l \tilde{\mu}_{l-1} - \tilde{\mu}_l| + \left| \sqrt{A_l^2 \tilde{\sigma}_{l-1}^2} - \tilde{\sigma}_l \right|,$$

where $\sqrt{\cdot}$ and $(\cdot)^2$ are applied elementwise.

Comparing Theorem 2 and Theorem 1, the former is tighter than the latter, as $R_{\max}^2/(1-\gamma)^2$ is in practice a lot larger than the corresponding terms in Theorem 2. For instance, the maximum realizable step reward of the HalfCheetah-v4 environment of the MuJoCo physics engine (Todorov et al., 2012) is around 11.7 (Hui et al., 2023). If the discount factor is chosen as $\gamma = 0.99$ following common practice, one would have, e.g., $R_{\max}^2/(1-\gamma)^2 = 1.37 \times 10^6$. Contrarily, the Lipschitz continuities of MLPs with two layers, used in the experiments, are much smaller and in the low hundreds (Khromov and Singh, 2024). Remarkably, Theorem 2 the bound makes an exact statement on the maximum possible value estimation error on a moment-matching MLP, as opposed to the high-probability bound presented in Theorem 1 for the sampling-based MLP. Hence, a sampling-based MLP would need a significantly large number of samples to match the tightness of the moment-matching MLP bound and only with high probability. We therefore expect our method to be more robust than sampling-based approaches, which is confirmed by our experimental results.

5 Experiments

We assess the performance of our model on twelve data sets of the D4RL offline RL benchmark (Fu et al., 2020). The D4RL dataset consists of data collected from three MuJoCo environments (halfcheetah, hopper, walker2d) with behavior policies having four degrees of expertise (random, medium, medium-replay, and medium-expert). We use the 'v2' versions of all data sets. To run the experiments, we use the official repository of MOBILE (Sun et al., 2023), in addition to our own model implementation, which is available at anonymous. Throughout the experiments, we follow MOBILE's configurations, with additional hyperparameter optimization. See Appendix C for details regarding the hyperparameters and experimental configurations.

We compare our model with the two main uncertainty-driven, model-based offline RL algorithms, namely MOPO (Yu et al., 2020), and MOBILE (Sun et al., 2023). These methods are considered the best representatives of model-based offline RL. They employ reward penalization based on state uncertainty (MOPO), and value uncertainty (MOBILE) respectively. MOBILE additionally serves as a representative of the state of the art in model-based offline RL in general. We obtain performance scores for the baseline models from log files provided by the OfflineRL library (Sun, 2023). As the

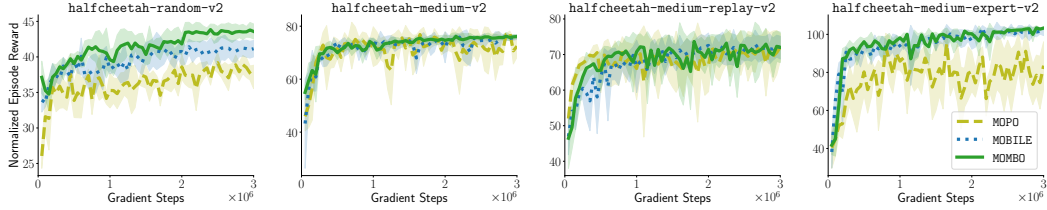


Figure 1: Evaluation results on `halfcheetah` for four settings. The dashed, dotted, and solid curves visualize the mean of the normalized rewards across ten evaluation episodes and four random seeds. The shaded area covers up to one standard deviation distance to the mean.

library does not provide log files for MOPO with `random` expertise, we reran them ourselves using the provided implementation and suggested hyperparameters.

Our results are summarized in Table 1. The performance of all three models is evaluated based on two metrics: the *normalized reward* and the learning efficiency, which is quantified using the *Area Under the Curve (AUC)*. The AUC score is calculated as the mean of the average normalized scores over ten evaluation episodes throughout the training process. The normalized score represents the performance of the algorithms in the final episode of training. To further illustrate these results, we provide a visualization of the evaluation curves for the `halfcheetah` environment in Figure 1. See Appendix D for larger versions of these four plots as well as for additional evaluation curve visualizations on the remaining environments.

Discussion and results. To summarize, our experimental findings are: (i) *MOMBO matches the state of the art MOBILE in normalized reward.* Additionally, it outperforms other model-based offline RL approaches like COMBO (Yu et al., 2021) with 66.8, TT (Janner et al., 2021) with 62.3, and RAMBO (Rigter et al., 2022) with 67.7 as their respective average normalized reward scores across the same twelve tasks. These numbers are cited from Sun et al. (2023). (ii) *MOMBO is more sample efficient.* It learns faster and reaches its final performance earlier. This is reflected in its AUC score, where MOMBO outperforms the baselines. (iii) *MOMBO is more robust.* It has a lower standard deviation of the normalized reward in six out of twelve tasks. This indicates better stability compared to MOBILE, which has a lower standard deviation in only three tasks. Note that for `hopper-random`, our model failed to learn in one repetition, leading to a high standard deviation and low average normalized reward. In conclusion, our MOMBO achieves state-of-the-art performance, exhibiting robustness and fast learning capabilities, aligning with the theory.

6 Conclusion

We introduced MOMBO, a novel method for model-based offline RL. The main objective of our method is to accurately quantify the uncertainty surrounding a Bellman target estimate caused by the error in the prediction of the next state. We achieve this by deterministically propagating uncertainties through the value function via moment matching and introducing pessimism by constructing LCB on the target Q-values. We analyze our model theoretically and evaluate its performance in various environments. Our findings may lay the groundwork for further theoretical analysis of model-based RL algorithms in continuous state-action spaces. Our algorithmic contributions can also be instrumental in both model-based online and model-free offline RL setups (An et al., 2021; Bai et al., 2022).

Limitations. The accuracy of the learned dynamics models sets a bottleneck on the performance of MOMBO. The choice of the confidence set radius β is also an overly decisive factor in model performance. MOMBO shares these two weaknesses with the other state-of-the-art model-based offline RL methods (Yu et al., 2020; Lu et al., 2021; Sun et al., 2023), however, does not contribute to their mitigation. Furthermore, our theoretical analyses are based on the assumption of normal distributed Q-values, which may be improved with heavy-tailed assumed densities. Considering the bounds, a limitation is that we claim a tighter bound compared to a baseline bound that we derived ourselves. However, the most important factor in that bound, $R_{\max}^2/(1-\gamma)^2$, arises via Hoeffding’s inequality, i.e., a classical statement. As such we assume our bound to be rigorous and not inadvertently biased. Finally, our moment matching method is limited to activation functions for which the first two

moments are either analytically tractable or can be approximated with sufficient accuracy. Extensions to transformations such as, e.g., BatchNorm (Ioffe and Szegedy, 2015), or other activation functions remove the analytical tractability of the current proposal. However, these are usually not used in our specific applications.

References

- Abbas, Z., Sokota, S., Talvitie, E., and White, M. (2020). Selective dyna-style planning under limited model capacity. In *International Conference on Machine Learning*.
- An, G., Moon, S., Kim, J., and Song, H. (2021). Uncertainty-based offline reinforcement learning with diversified q-ensemble. In *Advances in Neural Information Processing Systems*.
- Bai, C., Wang, L., Yang, Z., Deng, D., Garg, A., Liu, P., and Wang, Z. (2022). Pessimistic bootstrapping for uncertainty-driven offline reinforcement learning. In *International Conference on Learning Representations*.
- Cheng, C., Xie, T., Jiang, N., and Agarwal, A. (2022). Adversarially trained actor critic for offline reinforcement learning. In *International Conference on Machine Learning*.
- Chhachhi, S. and Teng, F. (2023). On the 1-wasserstein distance between location-scale distributions and the effect of differential privacy. *arXiv preprint arXiv:2304.14869*.
- Feinberg, V., Wan, A., Stoica, I., Jordan, M. I., Gonzalez, J., and Levine, S. (2018). Model-based value estimation for efficient model-free reinforcement learning. *arXiv preprint arXiv:1803.00101*.
- Frey, B. and Hinton, G. (1999). Variational learning in nonlinear gaussian belief networks. *Neural Computation*.
- Fu, J., Kumar, A., Nachum, O., Tucker, G., and Levine, S. (2020). D4rl: Datasets for deep data-driven reinforcement learning.
- Fujimoto, S. and Gu, S. (2021). A minimalist approach to offline reinforcement learning. In *Advances in Neural Information Processing Systems*.
- Fujimoto, S., Hoof, H., and Meger, D. (2018). Addressing function approximation error in actor-critic methods. In *International Conference on Machine Learning*.
- Fujimoto, S., Meger, D., and Precup, D. (2019). Off-policy deep reinforcement learning without exploration. In *International Conference on Machine Learning*.
- Gast, J. and Roth, S. (2018). Lightweight probabilistic deep networks. In *Conference on Computer Vision and Pattern Recognition*.
- Haarnoja, T., Zhou, A., Hartikainen, K., Tucker, G., Ha, S., Tan, J., Kumar, V., Zhu, H., Gupta, A., Abbeel, P., et al. (2018). Soft actor-critic algorithms and applications. *arXiv preprint arXiv:1812.05905*.
- Haußmann, M., Hamprecht, F., and Kandemir, M. (2019). Deep active learning with adaptive acquisition. In *Joint Conference on Artificial Intelligence*.
- Hoeffding, W. (1963). Probability inequalities for sums of bounded random variables. *Journal of the American Statistical Association*.
- Hui, D., Courville, A., and Bacon, P. (2023). Double gumbel q-learning. *Advances in Neural Information Processing Systems*.
- Ioffe, S. and Szegedy, C. (2015). Batch normalization: Accelerating deep network training by reducing internal covariate shift. In *International conference on machine learning*.
- Janner, M., Fu, J., Zhang, M., and Levine, D. (2019). When to trust your model: Model-based policy optimization. In *Advances in Neural Information Processing Systems*.
- Janner, M., Li, Q., and Levine, S. (2021). Offline reinforcement learning as one big sequence modeling problem. In *Advances in Neural Information Processing Systems*.
- Jeong, J., Wang, X., Gimelfarb, M., Kim, H., Abdulhai, B., and Sanner, S. (2023). Conservative bayesian model-based value expansion for offline policy optimization. In *International Conference on Learning Representations*.
- Jin, Y., Yang, Z., and Wang, Z. (2021). Is pessimism provably efficient for offline rl? In *International Conference on Machine Learning*.

- Khromov, G. and Singh, S. (2024). Some fundamental aspects about lipschitz continuity of neural networks. In *International Conference on Learning Representations*.
- Kidambi, R., Rajeswaran, A., Netrapalli, P., and Joachims, T. (2020). MORL : Model-based offline reinforcement learning. In *Advances in Neural Information Processing Systems*.
- Kingma, D. and Ba, J. (2015). Adam: A method for stochastic optimization. In *International Conference on Learning Representations*.
- Kostrikov, I., Fergus, R., Tompson, J., and Nachum, O. (2021). Offline reinforcement learning with fisher divergence critic regularization. In *International Conference on Machine Learning*.
- Kumar, A., Fu, J., Soh, M., Tucker, G., and Levine, S. (2019). Stabilizing off-policy q-learning via bootstrapping error reduction. In *Advances in Neural Information Processing Systems*.
- Kumar, A., Zhou, A., Tucker, G., and Levine, S. (2020). Conservative q-learning for offline reinforcement learning. In *Advances in Neural Information Processing Systems*.
- Lakshminarayanan, B., Pritzel, A., and Blundell, C. (2017). Simple and scalable predictive uncertainty estimation using deep ensembles. In *Advances in Neural Information Processing Systems*.
- Lange, S., Gabel, T., and Riedmiller, M. (2012). Batch reinforcement learning. In *Reinforcement learning: State-of-the-art*. Springer.
- Levine, S., Kumar, A., Tucker, G., and Fu, J. (2020). Offline reinforcement learning: Tutorial, review, and perspectives on open problems. *arXiv preprint arXiv:2005.01643*.
- Lu, C., Ball, P., Parker-Holder, J., Osborne, M., and Roberts, S. (2021). Revisiting design choices in offline model-based reinforcement learning. In *International Conference on Learning Representations*.
- Luis, C., Bottero, A., Vinogradskaya, J., Berkenkamp, F., and Peters, J. (2023). Model-based uncertainty in value functions. In *International Conference on Artificial Intelligence and Statistics*.
- Micheli, V., Alonso, E., and Fleuret, F. (2022). Transformers are sample-efficient world models. In *International Conference on Learning Representations*.
- Nie, X., Brunskill, E., and Wager, S. (2021). Learning when-to-treat policies. *Journal of the American Statistical Association*.
- O’Donoghue, B., Osband, I., Munos, R., and Mnih, V. (2018). The uncertainty bellman equation and exploration. In *International Conference on Machine Learning*.
- Peng, X., Kumar, A., Zhang, G., and Levine, S. (2019). Advantage-weighted regression: Simple and scalable off-policy reinforcement learning. *arXiv preprint arXiv:1910.00177*.
- Pitcan, Y. (2017). A note on concentration inequalities for u-statistics. *arXiv preprint arXiv:1712.06160*.
- Rigter, M., Lacerda, B., and Hawes, N. (2022). RAMBO-RL: Robust adversarial model-based offline reinforcement learning. In *Advances in Neural Information Processing Systems*.
- Shortreed, S. M., Laber, E., Lizotte, D., Stroup, T., Pineau, J., and Murphy, S. (2011). Informing sequential clinical decision-making through reinforcement learning: an empirical study. *Machine learning*.
- Siegel, S., Jost, T., Berkenkamp, F., Abdolmaleki, A., Neunert, M., Lampe, T., Hafner, R., Heess, N., and Riedmiller, M. (2020). Keep doing what worked: Behavior modelling priors for offline reinforcement learning. In *International Conference on Learning Representations*.
- Singh, A., Yu, A., Yang, J., Zhang, J., Kumar, A., and Levine, S. (2020). COG: Connecting new skills to past experience with offline reinforcement learning. In *Conference on Robot Learning*.
- Sun, Y. (2023). Offlinerl-kit: An elegant pytorch offline reinforcement learning library. <https://github.com/yihaosun1124/OfflineRL-Kit>.
- Sun, Y., Zhang, J., Jia, C., Lin, H., Ye, J., and Yu, Y. (2023). Model-bellman inconsistency for model-based offline reinforcement learning. In *International Conference on Machine Learning*.
- Sutton, R. (1990). Integrated architectures for learning, planning, and reacting based on approximating dynamic programming. In *Machine Learning Proceedings 1990*. Morgan Kaufmann.
- Sutton, R. and Barto, A. (2018). *Reinforcement learning: An introduction*. MIT press.

- Thrun, S. and Schwartz, A. (1993). Issues in using function approximation for reinforcement learning. In *Proceedings of the Fourth Connectionist Models Summer School*.
- Todorov, E., Erez, T., and Tassa, Y. (2012). Mujoco: A physics engine for model-based control. In *IEEE/RSJ International Conference on Intelligent Robots and Systems (IROS)*. IEEE.
- Uehara, M. and Sun, W. (2022). Pessimistic model-based offline reinforcement learning under partial coverage. In *International Conference on Learning Representations*.
- Villani, C. et al. (2009). *Optimal transport: old and new*. Springer.
- Wang, S. and Manning, C. (2013). Fast dropout training. In *International Conference on Machine Learning*.
- Wasserman, L. (2004). *All of Statistics*. Springer New York.
- Wu, A., Nowozin, S., Meeds, E., Turner, R., Hernandez-Lobato, J., and Gaunt, A. (2019a). Deterministic variational inference for robust bayesian neural networks. In *International Conference on Learning Representations*.
- Wu, Y., Tucker, G., and Nachum, O. (2019b). Behavior regularized offline reinforcement learning. *arXiv preprint arXiv:1911.11361*.
- Xie, T., Cheng, C., Jiang, N., Mineiro, P., and Agarwal, A. (2021). Bellman-consistent pessimism for offline reinforcement learning. *Advances in Neural Information Processing Systems*.
- Yu, T., Kumar, A., Rafailov, R., Rajeswaran, A., Levine, S., and Finn, C. (2021). COMBO: Conservative offline model-based policy optimization. In *Advances in Neural Information Processing Systems*.
- Yu, T., Thomas, G., Yu, L., Ermon, S., Zou, J., Levine, S., Finn, C., and Ma, T. (2020). MOPO: Model-based offline policy optimization. In *Advances in Neural Information Processing Systems*.

APPENDIX

A Related work

Offline RL. The goal of offline RL is to derive an optimal policy from fixed datasets collected through interactions with a behavioral policy in the environment. This approach is mostly relevant in scenarios where direct interaction with the environment is costly or poses potential risks. The applications of Offline RL span various domains, including robotics (Singh et al., 2020; Micheli et al., 2022) and healthcare (Shortreed et al., 2011; Nie et al., 2021). Notably, applying online off-policy RL algorithms directly to offline RL settings often fails due to issues such as overestimation bias and distributional shift. Research in Offline RL has evolved along two main avenues: model-free and model-based approaches.

Model-based offline RL. Dyna-style model-based RL (Sutton, 1990; Janner et al., 2019) algorithms employ a dynamics model to simulate the true transition model, which generates a synthetic dataset to enhance sample efficiency and serves as a surrogate environment for interaction. Model-based offline RL methods vary in their approach to applying conservatism using the dynamics model. For instance, MOPO (Yu et al., 2020) and MOREl (Kidambi et al., 2020) simply learn a pessimistic value function by penalizing the MDP generated by the dynamics model, with rewards being penalized based on different uncertainty measures of the dynamics model. COMBO (Yu et al., 2021) is a Dyna-style model-based approach derived from CQL (Kumar et al., 2020). RAMBO (Rigter et al., 2022) introduces conservatism by adversarially training the dynamics model to minimize the value function, thus ensuring accurate predictions. MOBILE (Sun et al., 2023) penalizes the value function based on the uncertainty of the Bellman operator through sampling. CBOP (Jeong et al., 2023) introduces conservatism by applying LCB to the value function with adaptive weighting of h -step returns in the model-based value expansion framework (Feinberg et al., 2018).

Uncertainty-driven offline RL. Uncertainty-driven offline RL approaches adhere to the meta-algorithm known as pessimistic value iteration (PEVI) (Jin et al., 2021). This meta-algorithm introduces pessimism through a ξ -uncertainty quantifier to minimize the Bellman error. In the realm of offline RL literature, practical implementations of this meta-algorithm exist for both model-free methods, such as EDAC (An et al., 2021) and PBRL (Bai et al., 2022), and model-based approaches like MOPO (Yu et al., 2020) and MOBILE (Sun et al., 2023). PBRL constructs its ξ -uncertainty quantifier based on the disagreement among bootstrapped Q-functions, while EDAC incorporates uncertainty from ensemble value functions. Model-based versions of these methods construct their ξ -uncertainty quantifiers using information from the dynamics model. For instance, MOPO leverages prediction uncertainty from the dynamics model in various ways, as explored by Lu et al. (2021), while MOBILE uses uncertainty in the value function for the synthetic dataset by sampling. Our model, MOMBO, also implements PEVI, and our ξ -uncertainty quantifier is based on the uncertainty of the target Q-value, which does not rely on sampling. Instead, it directly propagates uncertainty from the dynamics models to the value function thanks to moment matching.

Model-free offline RL. Model-free offline RL algorithms can be broadly categorized into two groups: policy regularization and value regularization. Policy regularization methods aim to constrain the learned policy to prevent deviations from the behavioral policy (Fujimoto et al., 2019; Kumar et al., 2019; Wu et al., 2019b; Peng et al., 2019; Siegel et al., 2020). For instance, during training, TD3-BC (Fujimoto and Gu, 2021) incorporates a behavior cloning term to regulate its policy. On the other hand, value regularization methods (Kostrikov et al., 2021; Xie et al., 2021; Cheng et al., 2022) introduce conservatism during the value optimization phase using various approaches. For example, CQL (Kumar et al., 2020) penalizes Q-values associated with OOD actions to avoid overestimation. Similarly, EDAC (An et al., 2021), employing ensemble value networks, applies a similar penalization strategy based on uncertainty measures over Q-values.

Uncertainty propagation. Uncertainty propagation via varying moment matching-based approaches has been well-researched primarily in the area of Bayesian deep learning (Frey and Hinton, 1999; Wang and Manning, 2013; Wu et al., 2019a), with applications, e.g., in active learning (Haußmann et al., 2019) and computer vision (Gast and Roth, 2018).

B Proofs

This section contains proofs for all theoretical statements made in the main text.

Lemma 1 (*Moment matching*). For $X \sim \mathcal{N}(X|\mu, \sigma^2)$ and $Y = \max(0, X)$, we have

$$(i) \quad \begin{aligned} \tilde{\mu} &\triangleq \mathbb{E}[Y] = \mu\Phi(\alpha) + \sigma\phi(\alpha), \\ \tilde{\sigma}^2 &\triangleq \text{var}[Y] = (\mu^2 + \sigma^2)\Phi(\alpha) + \mu\sigma\phi(\alpha) - \tilde{\mu}^2, \end{aligned}$$

where $\alpha = \mu/\sigma$, and $\phi(\cdot)$, $\Phi(\cdot)$ are the probability density function (pdf) and cumulative distribution function (cdf) of the standard normal distribution, respectively. Additionally, we have that

$$(ii) \quad \tilde{\mu} \geq \mu \quad \text{and} \quad (iii) \quad \tilde{\sigma}^2 \leq \sigma^2.$$

Proof of Lemma 1. See [Frey and Hinton \(1999\)](#) for a derivation of (i), i.e., $\tilde{\mu}$ and $\tilde{\sigma}^2$.

Statement (ii) holds as

$$\tilde{\mu} = \mathbb{E}[Y] = \int_0^\infty xp(x)dy \geq \int_{-\infty}^0 xp(x)dx + \int_0^\infty xp(x)dx = \mu.$$

Note that

$$\mathbb{E}[Y^2] = \int_0^\infty x^2p(x)dx \leq \int_{-\infty}^0 x^2p(x)dx + \int_0^\infty x^2p(x)dx = \mathbb{E}[X^2].$$

Therefore, we get (iii) by

$$\tilde{\sigma}^2 = \text{var}[Y] = \mathbb{E}[Y^2] - \tilde{\mu}^2 \leq \mathbb{E}[X^2] - \mu^2 = \sigma^2,$$

concluding the proof. \square

Lemma 2 (*An inequality between normal cdfs*) For two normally distributed random variables $X \sim \mathcal{N}(X|\mu, \sigma^2)$ and $\tilde{X} \sim \mathcal{N}(\tilde{X}|\tilde{\mu}, \tilde{\sigma}^2)$ with $\tilde{\mu}\sigma \geq \mu\tilde{\sigma}$, the following inequality holds:

$$F_{\tilde{X}}(u) \leq F_X(u), \quad \text{for } u \leq 0.$$

Proof of Lemma 2. Assume $u \leq 0$. We have that

$$F_{\tilde{X}}(u) \leq F_X(u) \quad \Leftrightarrow \quad \Phi\left(\frac{u - \tilde{\mu}}{\tilde{\sigma}}\right) \leq \Phi\left(\frac{u - \mu}{\sigma}\right),$$

where $\Phi(x) = \frac{1}{\sqrt{2\pi}} \int_{-\infty}^x \exp(-t^2/2) dt$ is the cumulative distribution function (cdf) of the standard normal distribution. As it monotonically increases, this in turn is equivalent to

$$\begin{aligned} \frac{u - \tilde{\mu}}{\tilde{\sigma}} \leq \frac{u - \mu}{\sigma} &\Leftrightarrow u\sigma - \tilde{\mu}\sigma \leq u\tilde{\sigma} - \mu\tilde{\sigma} \\ &\Leftrightarrow u(\sigma - \tilde{\sigma}) \leq \tilde{\mu}\sigma - \mu\tilde{\sigma} \end{aligned}$$

which holds as $u(\sigma - \tilde{\sigma}) < 0$ via Lemma 1 for $u < 0$, and $\tilde{\mu}\sigma \geq \mu\tilde{\sigma}$ by assumption. \square

Lemma 3 (*Wasserstein inequalities*). The following inequalities hold for the 1-Wasserstein metric

- (i) $W_1(\rho_U^1, \rho_U^2) \leq \|A\|_1 W_1(\rho_V^1, \rho_V^2)$, for $U = AV + b$, where $\|\cdot\| \triangleq \|\cdot\|_1$ is the 1-norm.
- (ii) $W_1(\rho_Z^1, \rho_Z^2) \leq W_1(\rho_U^1, \rho_U^2)$, for $Z = f(U)$ with $f(\cdot)$ locally K -Lipschitz with $K \leq 1$,

where ρ_x is the density of x , $U \in \mathbb{R}^{d_u}$, $V \in \mathbb{R}^{d_v}$, $A \in \mathbb{R}^{d_u \times d_v}$, and $b \in \mathbb{R}^{d_u}$.

Proof of Lemma 3. Given the Kantorovich-Rubinstein duality ([Villani et al., 2009](#)) for W_1 we have

$$W_1(\mu, \nu) = \frac{1}{K} \sup_{\|f\|_L \leq K} \mathbb{E}_{x \sim \mu} [f(x)] - \mathbb{E}_{y \sim \nu} [f(y)],$$

for any two probability measures μ, ν , with $K > 0$ and $\|\cdot\|_L$ is the L -Lipschitz norm.

This gives us for $K = 1$ and $Y = g(X)$ that

$$\begin{aligned} W_1(\mu_Y, \nu_Y) &= \sup_{\|f\|_L \leq 1} \mathbb{E}_{y \sim \mu_Y} [f(y)] - \mathbb{E}_{y \sim \nu_Y} [f(y)] \\ &= \sup_{\|f\|_L \leq 1} \mathbb{E}_{x \sim \mu_X} [f(g(x))] - \mathbb{E}_{x \sim \nu_X} [f(g(x))], && \text{change of variables} \\ &\leq \sup_{\|h\|_L \leq 1} \mathbb{E}_{x \sim \mu_X} [h(x)] - \mathbb{E}_{x \sim \nu_X} [h(x)] = W_1(\mu_X, \nu_X) \end{aligned}$$

where the inequality holds as $f \circ g$ has a Lipschitz constant $L \leq 1$, i.e., we end up with a supremum over a smaller class of Lipschitz functions which we revert in the inequality. This gives us (ii). We get (i) analogously for $|A| \leq 1$ and for $|A| > 1$ via $K = |A|$. \square

Lemma 4 (*W_1 Bound on an MLP*). Consider a multi-layer perceptron (MLP) $f(\cdot)$ with L layers

$$Y_l = A_l^\top X_{l-1} + b_l, \quad X_l = r(Y_l) \quad l = 1, \dots, L,$$

where A_l, b_l are the weight matrix and bias vector for layer l , and $r(\cdot)$ denotes an elementwise 1-Lipschitz activation function. We write $Y \triangleq Y_L = f(X_0)$, where X_0 is the input. Assuming two measures $X_1 \sim \rho_X^1$ and $X_2 \sim \rho_X^2$, we have that

$$W_1(\rho_Y^1, \rho_Y^2) \leq \prod_{l=1}^L \|A_l\| W_1(\rho_X^1, \rho_X^2).$$

Proof of Lemma 4. We have that

$$\begin{aligned} W_1(\rho_Y^1, \rho_Y^2) &\leq |A_L| W_1(\rho_{X_{L-1}}^1, \rho_{X_{L-1}}^2), && \text{via Lemma 3 (i)} \\ &= |A_L| W_1(\rho_{h(Y_{L-1})}^1, \rho_{h(Y_{L-1})}^2) \leq |A_L| W_1(\rho_{Y_{L-1}}^1, \rho_{Y_{L-1}}^2), && \text{via Lemma 3 (ii)} \\ &\leq \dots \leq \prod_{l=1}^L \|A_l\| W_1(\rho_X^1, \rho_X^2). \end{aligned}$$

\square

Lemma 5 (*Moment-matching bound*). For the following three random variables

$$X \sim \rho_X, \quad Y = \max(0, X), \quad \tilde{X} \sim \mathcal{N}(\tilde{X} | \tilde{\mu}, \tilde{\sigma}^2),$$

with $\tilde{\mu} = \mathbb{E}[Y]$ and $\tilde{\sigma}^2 = \text{var}[Y]$ the following inequality holds

$$W_1(\rho_Y, \rho_{\tilde{X}}) \leq \int_{-\infty}^0 F_{\tilde{X}}(u) du + W_1(\rho_X, \rho_{\tilde{X}}).$$

If $\rho_X = \mathcal{N}(X | \mu, \sigma)$, it can be further simplified to

$$W_1(\rho_Y, \rho_{\tilde{X}}) \leq \tilde{\sigma} \phi\left(\frac{\tilde{\mu}}{\tilde{\sigma}}\right) - \tilde{\mu} \Phi\left(-\frac{\tilde{\mu}}{\tilde{\sigma}}\right) + |\mu - \tilde{\mu}| + |\sigma - \tilde{\sigma}|.$$

where $\Phi(\cdot)$ is the cdf of a standard normal distribution.

Proof of Lemma 5. For a generic $X \sim \rho_X$, $Y = \max(0, X)$ and $\tilde{X} \sim \mathcal{N}(\tilde{\mu}, \tilde{\sigma}^2)$, we have with $F_Y(u) = \mathbb{1}_{u \geq 0} F_X(u)$ ¹ and (7) that

$$\begin{aligned} W_1(\rho_Y, \rho_{\tilde{X}}) &= \int_{\mathbb{R}} |F_Y(u) - F_{\tilde{X}}(u)| du \\ &= \int_{-\infty}^0 F_{\tilde{X}}(u) du + \int_0^{\infty} |F_X(u) - F_{\tilde{X}}(u)| du \end{aligned}$$

¹The indicator function $\mathbb{1}$ is defined as $\mathbb{1}_S = 1$ if the statement S is true and 0 otherwise.

$$\begin{aligned}
&\leq \int_{-\infty}^0 F_{\tilde{X}}(u)du + \int_0^\infty |F_X(u) - F_{\tilde{X}}(u)|du + \int_{-\infty}^0 |F_X(u) - F_{\tilde{X}}(u)|du \\
&= \int_{-\infty}^0 F_{\tilde{X}}(u)du + W_1(\rho_X, \rho_{\tilde{X}}).
\end{aligned}$$

If $\rho_X = \mathcal{N}(X|\mu, \sigma)$, we can upper bound the W_1 distance as (Chhachhi and Teng, 2023)

$$W_1(\mathcal{N}(\mu_1, \sigma_1^2), \mathcal{N}(\mu_2, \sigma_2^2)) \leq |\mu_1 - \mu_2| + |\sigma_1 - \sigma_2|,$$

and evaluate the integral as

$$\int_{-\infty}^0 F_{\tilde{X}}(u)du = \int_{-\infty}^0 \Phi\left(\frac{u - \tilde{\mu}}{\tilde{\sigma}}\right) du = \tilde{\sigma}\phi\left(\frac{\tilde{\mu}}{\tilde{\sigma}}\right) - \tilde{\mu}\Phi\left(-\frac{\tilde{\mu}}{\tilde{\sigma}}\right),$$

where we used that

$$\int \Phi(a + bx)dx = \frac{1}{b}((a + bx)\Phi(a + bx) + \phi(a + bx)) + C,$$

where C is a constant. Together this gives us that

$$W_1(\rho_Y, \rho_{\tilde{Y}}) \leq \sigma\phi\left(\frac{\tilde{\mu}}{\tilde{\sigma}}\right) - \tilde{\mu}\Phi\left(-\frac{\tilde{\mu}}{\tilde{\sigma}}\right) + |\mu - \tilde{\mu}| + |\sigma - \tilde{\sigma}|.$$

□

Theorem 1 (Sampling-based MLP bound). For an L layer MLP $f(\cdot)$ as defined in Lemma 4, with $Y \triangleq Y_L = f(X)$ where $X \sim \mathcal{N}(X|\mu_X, \sigma_X^2)$, the following bound holds:

$$\mathbb{P}\left(W_1(\rho_Y, \rho_{\hat{Y}}^N) \leq \prod_{l=1}^L \|A_l\| \sqrt{-\frac{8 \log(\delta/4) R_{\max}^2}{\lfloor N/2 \rfloor (1 - \gamma)^2}}\right) \geq 1 - \delta.$$

where $\delta \in (0, 1)$ and $\hat{\rho}_Y^N$ is the empirical estimate given N i.i.d. samples.

Proof of Theorem 1. With Hoeffding's inequality (Wasserman, 2004), we have that

$$\mathbb{P}(|\hat{\mu}_N - \mu| \geq \varepsilon) \leq 2 \exp\left(-\frac{2\varepsilon^2}{\sum_{i=1}^n (\frac{R_{\max}}{1-\gamma} - 0)^2}\right) = 2 \exp\left(-\frac{2\varepsilon^2 N(1-\gamma)^2}{R_{\max}^2}\right),$$

for the empirical mean $\hat{\mu}_N$ of Y . As variances are U-statistics with order $m = 2$ and kernel $h = \frac{1}{2}(x - y)^2$ using Hoeffding (1963); Pitcan (2017), we have for the empirical covariance of Y , $\hat{\sigma}_N^2$, that

$$\begin{aligned}
\mathbb{P}(\hat{\sigma}_N^2 - \sigma^2 \geq \varepsilon) &\leq \exp\left(-\frac{\varepsilon^2 \lfloor N/m \rfloor}{2\|h\|_\infty^2}\right) = \exp\left(-\frac{\varepsilon^2 \lfloor N/2 \rfloor (1-\gamma)^2}{2R_{\max}^2}\right) \\
\Leftrightarrow \mathbb{P}(\hat{\sigma}_N^2 - \sigma^2 \leq \varepsilon) &\geq 1 - \exp\left(-\frac{\varepsilon^2 \lfloor N/2 \rfloor (1-\gamma)^2}{2R_{\max}^2}\right)
\end{aligned}$$

Applying the inequality $\hat{\sigma}_N \leq \sqrt{\sigma^2 + \varepsilon} \leq \sigma + \sqrt{\varepsilon}$, we get

$$\begin{aligned}
\mathbb{P}(\hat{\sigma}_N \leq \sigma + \varepsilon) &\geq 1 - \exp\left(-\frac{\varepsilon^2 \lfloor N/2 \rfloor (1-\gamma)^2}{2R_{\max}^2}\right) \\
\Leftrightarrow \mathbb{P}(\hat{\sigma}_N - \sigma \geq \varepsilon) &\leq \exp\left(-\frac{\varepsilon^2 \lfloor N/2 \rfloor (1-\gamma)^2}{2R_{\max}^2}\right).
\end{aligned}$$

As the same inequality holds for $\sigma - \hat{\sigma}_N \geq \varepsilon$, a union bound give us that

$$\mathbb{P}(|\sigma - \hat{\sigma}_N| \geq \varepsilon) \leq 2 \exp\left(-\frac{\varepsilon^2 \lfloor N/2 \rfloor (1-\gamma)^2}{2R_{\max}^2}\right).$$

Using an analytical upper bound (Chhachhi and Teng, 2023) on the Wasserstein-1 distance between two normal distributions,

$$W_1(\mathcal{N}(\mu_1, \sigma_1^2), \mathcal{N}(\mu_2, \sigma_2^2)) \leq |\mu_1 - \mu_2| + |\sigma_1 - \sigma_2|,$$

we have that

$$\begin{aligned} \mathbb{P}(W_1(\mathcal{N}(\mu, \sigma^2), \mathcal{N}(\hat{\mu}_N, \hat{\sigma}_N)) \geq 2\varepsilon) &\leq \mathbb{P}(|\mu - \hat{\mu}_N| + |\sigma - \hat{\sigma}_N| \geq 2\varepsilon) \\ &\leq \mathbb{P}(|\hat{\mu}_N - \mu| \geq \varepsilon \text{ or } |\hat{\sigma}_N - \sigma| \geq \varepsilon) \leq \mathbb{P}(|\hat{\mu}_N - \mu| \geq \varepsilon) + \mathbb{P}(|\hat{\sigma}_N - \sigma| \geq \varepsilon), && \text{union bound} \\ &\leq 2 \exp(-2Nc\varepsilon^2) + 2 \exp(-0.5 \lfloor N/2 \rfloor c\varepsilon^2) \leq 4 \exp(-0.5 \lfloor N/2 \rfloor c\varepsilon^2) \triangleq \delta, && c \triangleq (1 - \gamma)^2 / R_{\max}^2. \end{aligned}$$

Solving for $\bar{\varepsilon} = 2\varepsilon$ gives us

$$\bar{\varepsilon} = \sqrt{-\frac{8 \log(\delta/4)}{\lfloor N/2 \rfloor c}}.$$

The bound is then given as

$$\mathbb{P}\left(W_1(\mathcal{N}(\mu, \sigma^2), \mathcal{N}(\hat{\mu}_N, \hat{\sigma}_N^2)) \leq \sqrt{-\frac{8 \log(\delta/4)}{\lfloor N/2 \rfloor c}}\right) \geq 1 - \delta,$$

which gives us with Lemma 4, that

$$\mathbb{P}\left(W_1(\rho_Y, \rho_Y^N) \leq \prod_{l=1}^L \|A_l\| \sqrt{-\frac{8 \log(\delta/4) R_{\max}^2}{\lfloor N/2 \rfloor (1 - \gamma)^2}}\right) \geq 1 - \delta.$$

□

Theorem 2 (Moment-matching MLP bound). *Let $f(X)$, be an MLP with L fully connected layers, and ReLU activation $r(x) = \max(0, x)$. For $l = 1, \dots, L - 1$, the sampling-based forward-pass is*

$$Y_0 = X_s, \quad Y_l = r(f_l(Y_{l-1})), \quad Y_L = f_L(Y_{L-1}),$$

where $f_l(\cdot)$ is the l -th layer and X_s a sample of $\mathcal{N}(X|\mu_X, \sigma_X^2)$. Its moment matching pendant is

$$\tilde{X}_0 \sim \mathcal{N}(\tilde{X}_0|\mu_X, \sigma_X^2), \quad \tilde{X}_l \sim \mathcal{N}\left(\tilde{X}_l \mid \mathbb{E}\left[r(f_l(\tilde{X}_{l-1}))\right], \text{var}\left[r(f_l(\tilde{X}_{l-1}))\right]\right).$$

The following inequality holds for $\tilde{\rho}_Y = \rho_{\tilde{X}_L} = \mathcal{N}(\tilde{X}_L|\mathbb{E}[f(\tilde{X}_{L-1})], \text{var}[f(\tilde{X}_{L-1})])$.

$$W_1(\rho_Y, \tilde{\rho}_Y) \leq \sum_{l=2}^L \left(G(\tilde{X}_{l-1}) + C_{l-1}\right) \prod_{j=l}^L \|A_j\|,$$

with

$$G(\tilde{X}_l) = \tilde{\sigma}_l \phi\left(\frac{\tilde{\mu}_l}{\tilde{\sigma}_l}\right) - \tilde{\mu}_l \Phi\left(-\frac{\tilde{\mu}_l}{\tilde{\sigma}_l}\right) \leq 1, \quad C_l \leq |A_l \tilde{\mu}_{l-1} - \tilde{\mu}_l| + \left|\sqrt{A_l^2 \tilde{\sigma}_{l-1}^2} - \tilde{\sigma}_l\right|,$$

where $\sqrt{\cdot}$ and $(\cdot)^2$ are applied elementwise.

Proof of Theorem 2. Using Lemma 5 we have that the W_1 distance between the deterministic forward pass ρ_{Y_l} and the matching-based forward pass $\rho_{\tilde{X}_l}$ is given as

$$\begin{aligned} W_1(\rho_{Y_l}, \rho_{\tilde{X}_l}) &\leq G(\tilde{X}_l) + W_1(\rho_{f_l(Y_{l-1})}, \rho_{\tilde{X}_l}), && \text{where } G(X) \triangleq \int_{-\infty}^0 F_X(u) du \\ &\leq G(\tilde{X}_l) + W_1(\rho_{f_l(Y_{l-1})}, \rho_{f_l(\tilde{X}_{l-1})}) \\ &\quad + W_1(\rho_{f_l(\tilde{X}_{l-1})}, \rho_{\tilde{X}_l}), && \text{via the triangle inequality} \\ &\leq G(\tilde{X}_l) + \|A_l\| W_1(\rho_{Y_{l-1}}, \rho_{\tilde{X}_{l-1}}) + C_l && C_l \triangleq W_1(\rho_{f_l(\tilde{X}_{l-1})}, \rho_{\tilde{X}_l}) \\ &\leq G(\tilde{X}_l) + \|A_l\| \left(G(\tilde{X}_{l-1}) \right) \end{aligned}$$

$$+ \|A_{l-1}\|W_1(\rho_{Y_{l-2}}, \rho_{\tilde{X}_{l-2}}) + C_{l-1}) + C_l$$

I.e., for the whole MLP we have

$$\begin{aligned} W_1(\rho_Y, \tilde{\rho}_Y) &= W_1(\rho_{Y_L}, \rho_{\tilde{X}_L}) = \|A_L\|W_1(\rho_{Y_{L-1}}, \rho_{\tilde{X}_{L-1}}) \\ &\leq \|A_L\| \left(G(\tilde{X}_{L-1}) + \|A_{L-1}\|W_1(\rho_{Y_{L-2}}, \rho_{\tilde{X}_{L-2}}) + C_{L-1} \right) \\ &\leq \sum_{l=3}^L \left(G(\tilde{X}_{l-1}) + C_{l-1} \right) \prod_{j=l}^L \|A_j\| + W_1(\rho_{Y_1}, \rho_{\tilde{X}_1}) \prod_{l=2}^L \|A_l\|, \end{aligned}$$

where, finally,

$$W_1(\rho_{Y_1}, \rho_{\tilde{X}_1}) \leq \sigma\phi\left(\frac{\tilde{\mu}}{\tilde{\sigma}}\right) - \tilde{\mu}\Phi\left(-\frac{\tilde{\mu}}{\tilde{\sigma}}\right) + |A_1\mu_X - \tilde{\mu}_1| + \left| \sqrt{A_1^2\sigma_X^2} - \tilde{\sigma}_1 \right|.$$

$G(\tilde{X}_l)$ and C_l are given as

$$\begin{aligned} G(\tilde{X}_l) &= \tilde{\sigma}_l\phi\left(\frac{\tilde{\mu}_l}{\tilde{\sigma}_l}\right) - \tilde{\mu}_l\Phi\left(-\frac{\tilde{\mu}_l}{\tilde{\sigma}_l}\right), \\ C_l &\leq |A_l\tilde{\mu}_{l-1} - \tilde{\mu}_l| + \left| \sqrt{A_l^2\tilde{\sigma}_{l-1}^2} - \tilde{\sigma}_l \right|, \end{aligned}$$

where $\sqrt{\cdot}$ and $(\cdot)^2$ are applied elementwise. □

C Experimental details

C.1 Hyperparameters and experimental setup

In this section, we provide all the necessary details to reproduce our method. We evaluate our model with four repetitions using the following seeds: [0, 1, 2, 3]. We run the experiments using the official repository of MOBILE (Sun et al., 2023),² as well as our own model implementation, available at anonymous.

C.1.1 Dynamics model training

Following prior works (Yu et al., 2020, 2021; Sun et al., 2023), we model the transition model T as an ensemble of neural networks that predict the next state and reward as a Gaussian distribution. We formulate this as $\hat{T}_\theta(s', r) = \mathcal{N}(\mu_\theta(s, a), \Sigma_\theta(s, a))$, where μ_θ and Σ_θ are neural networks that model the parameters of the Gaussian distribution. These neural networks are parameterized with θ . Note that we learn a diagonal covariance $\Sigma_\theta(a, s)$.

We use $N_{\text{ens}} = 7$ ensemble elements and select $N_{\text{elite}} = 5$ elite elements from the ensemble based on a validation dataset containing 1000 transitions. Each model in the ensemble is a 4-layer feedforward neural network with 200 hidden units, and $L2$ weight decay is applied with the following weights for each layer, starting from the first layer: $[2.5 \times 10^{-5}, 5 \times 10^{-5}, 7.5 \times 10^{-5}, 7.5 \times 10^{-5}, 1 \times 10^{-4}]$. The dynamics model is trained using Maximum Likelihood Estimation with a learning rate of 0.001, a batch size of 256, and early stopping is applied for 5 steps using the validation dataset. The only exception is for walker2d-medium dataset, which has a fixed number of 30 learning episodes. We use Adam optimizer (Kingma and Ba, 2015) for the dynamics model.

Note that, to minimize differences and reduce training time, we use the pre-trained dynamics models provided in Sun (2023), specifically those from MOBILE.

C.1.2 Policy training

Architecture and optimization details. Our model is trained over 3000 episodes, with updates to the policy and Q-function performed 1000 times per episode, using a batch size of 256. The learning rate for the critic is set to 0.0003, while for the actor, it is 0.0001. We use Adam optimizer (Kingma

²<https://github.com/yihaosun1124/mobile/tree/4882dce878f0792a337c0a95c27f4abf7e926101>

Table 2: Hyperparameters for MOMBO.

Dataset Type	Environment	Rollout Length k	Penalty Coefficient β
random	halfcheetah	5	0.5
	hopper	5	4.5
	walker2d	5	2.5
medium	halfcheetah	5	0.75
	hopper	5	3.0
	walker2d	5	0.75
medium-replay	halfcheetah	5	0.2
	hopper	5	0.15
	walker2d	1	0.5
medium-expert	halfcheetah	5	1.0
	hopper	5	1.5
	walker2d	1	1.5

and Ba, 2015) for both actor and critics. We employ a cosine annealing learning rate scheduler for the actor. Both the actor and critic architectures consist of 2-layer feedforward neural networks with 256 hidden units. Unlike other baselines, our critic network is capable of deterministically propagating uncertainties via moment matching. The critic ensemble consists of two networks.

For policy optimization, we mostly follow the Soft Actor-Critic (SAC) (Haarnoja et al., 2018), with a difference in the policy evaluation phase. Using MOBILE’s configuration, we apply the deterministic Bellman backup operator instead of the soft Bellman backup operator. We set the discount factor to $\gamma = 0.99$ and the soft update parameter to $\tau = 0.005$. The α parameter is learned during training with the learning rate of 0.0001, except for `hopper-medium` and `hopper-medium-replay`, where $\alpha = 0.2$. The target entropy is set to $-\dim(\mathcal{A})$, where \dim is the number of dimensions.

Both the policy and actor are trained using a random mixture of the real dataset \mathcal{D} and synthetically generated rollouts $\hat{\mathcal{D}}$ with probabilities p and $1 - p$, respectively. The real ratio $p = 0.05$, except for `halfcheetah-medium-expert`, where $p = 0.5$.

Synthetic dataset generation for policy optimization. We follow the same procedure for synthetic dataset generation as is common in the literature. During this phase, a batch of initial states is sampled from the real dataset \mathcal{D} , and the corresponding actions are taken by the current policy. For each state-action pair in the batch, the dynamics models predict a Gaussian distribution over the next state and reward. One of the elite elements from the ensemble is chosen at random, and a sample is drawn from the predictive distribution for the next state and reward. These rollout transitions are stored in a synthetic dataset $\hat{\mathcal{D}}$. New rollouts are generated at the beginning of each episode and appended to $\hat{\mathcal{D}}$. The batch size for rollouts is set to 50000, and only the rollouts from the last 5 episodes are stored in $\hat{\mathcal{D}}$. The rollout lengths (k) for each task are shown in Table 2.

Hyperparameters: We adopted all configurations from MOBILE with the exception of β due to differences in the scale of the uncertainty estimators. Our choices for β and rollout length k for our model are provided in Table 2.

Time complexity. To propagate uncertainties through a neural network, we propagate the first two moments through the network, as shown in Algorithm 1. This procedure involves passing through the linear layer twice, once for the first moment and once for the second moment, along with some additional operations whose computation time is negligible. In contrast, sampling-based methods require N forward passes where N is the number of samples. Therefore, any $N \geq 2$ creates a computational overhead for sampling-based methods; for instance, $N = 10$ for MOBILE.

Experiment compute resources. We perform our experiments on three computational resources: 1) Tesla V100 GPU, Intel(R) Xeon(R) Gold 6230 CPU at 2.10 GHz, and 46 GB of memory; 2) NVIDIA Tesla A100 GPU, AMD EPYC 7F72 CPU at 3.2 GHz, and 256 GB of memory; and 3)

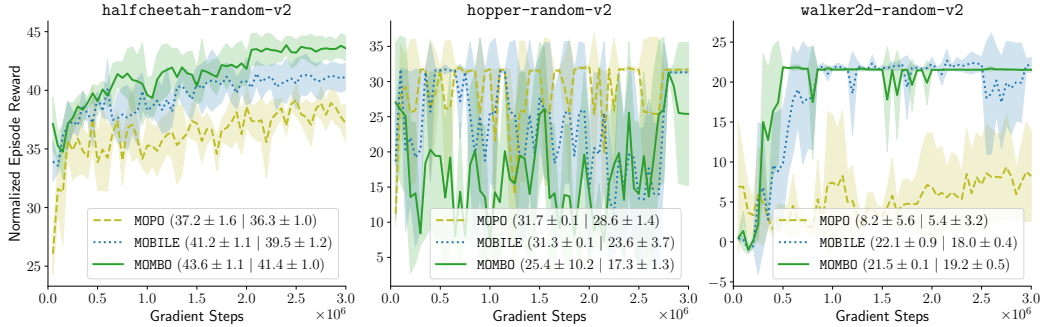


Figure 2: Evaluation results of uncertainty-driven model-based offline RL algorithms on random datasets: left panel halfcheetah, middle panel hopper, and right panel walker2d. The horizontal axis depicts the gradient steps, and the vertical axis shows the normalized episode reward. The thick (dashed/dotted/solid) curve represents the mean of the normalized rewards across ten evaluation episodes and four random seeds. The shaded area indicates one standard deviation from the mean. We also report the mean and standard deviation of the normalized reward and AUC score in the legend in this order.

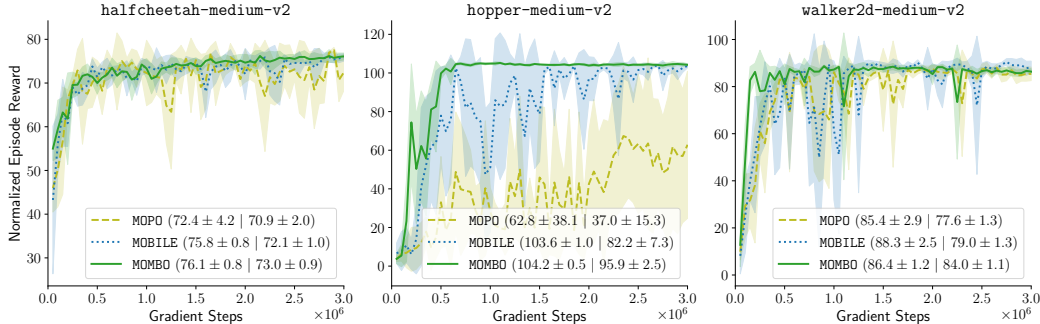


Figure 3: Evaluation results of uncertainty-driven model-based offline RL algorithms on medium datasets: left panel halfcheetah, middle panel hopper, and right panel walker2d. The horizontal axis depicts the gradient steps, and the vertical axis shows the normalized episode reward. The thick (dashed/dotted/solid) curve represents the mean of the normalized rewards across ten evaluation episodes and four random seeds. The shaded area indicates one standard deviation from the mean. We also report the mean and standard deviation of the normalized reward and AUC score in the legend in this order.

GeForce RTX 4090 GPU, Intel(R) Core(TM) i7-14700K CPU at 5.6 GHz, and 96 GB of memory. We measure the computation time for 1000 gradient steps as approximately 8 seconds on the third device, which would require approximately 330 hours of computation for all the repetitions of MOMBO, assuming the dynamics models are provided.

D Further results

Performance of the uncertainty-driven model-based offline RL approaches and ours through gradient steps are provided in Figures 2 to 5.

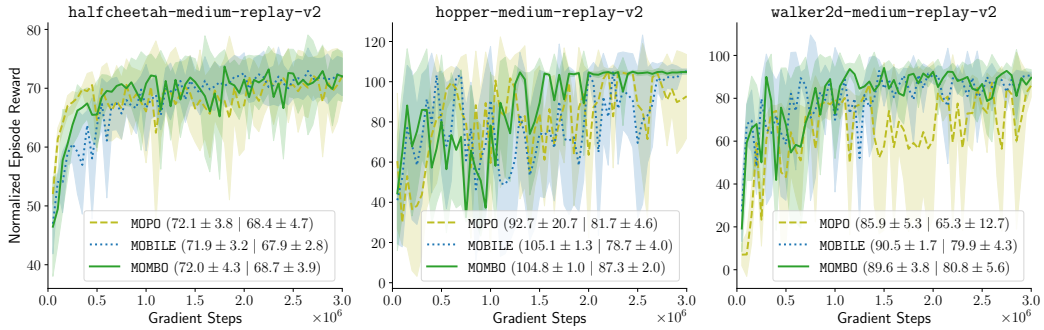


Figure 4: Evaluation results of uncertainty-driven model-based offline RL algorithms on medium-replay datasets: left panel halfcheetah, middle panel hopper, and right panel walker2d. The horizontal axis depicts the gradient steps, and the vertical axis shows the normalized episode reward. The thick (dashed/dotted/solid) curve represents the mean of the normalized rewards across ten evaluation episodes and four random seeds. The shaded area indicates one standard deviation from the mean. We also report the mean and standard deviation of the normalized reward and AUC score in the legend in this order.

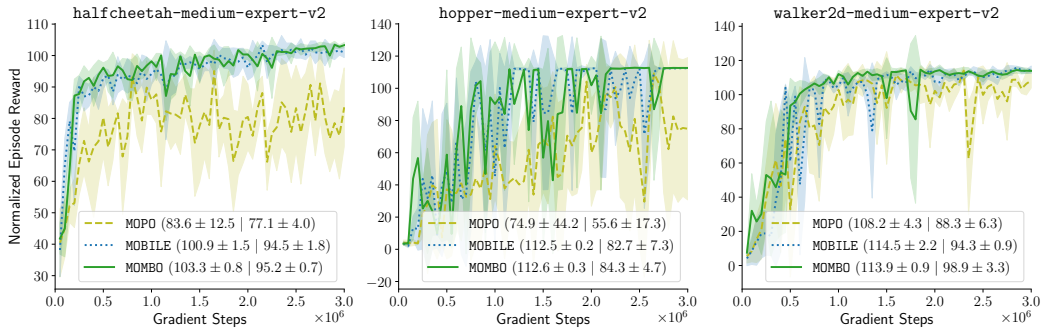


Figure 5: Evaluation results of uncertainty-driven model-based offline RL algorithms on medium-expert datasets: left panel halfcheetah, middle panel hopper, and right panel walker2d. The horizontal axis depicts the gradient steps, and the vertical axis shows the normalized episode reward. The thick (dashed/dotted/solid) curve represents the mean of the normalized rewards across ten evaluation episodes and four random seeds. The shaded area indicates one standard deviation from the mean. We also report the mean and standard deviation of the normalized reward and AUC score in the legend in this order.